Experimental and Computational Study of the OH−Isoprene Reaction: Isomeric Branching and Low-Pressure Behavior

W. Sean McGivern,[†] Inseon Suh,[‡] Angela D. Clinkenbeard,[‡] Renyi Zhang,[‡] and Simon W. North*[,†]

Department of Chemistry, Texas A&M University, P.O. Box 30012, College Station, Texas 77842, and Department of Atmospheric Sciences, Texas A&M University, College Station, Texas, 77842

Received: March 28, 2000; In Final Form: May 4, 2000

The kinetics of the isoprene−OH reaction have been studied both experimentally and computationally. Experimental rate constants at pressures in the range 0.5−20 Torr have been determined at 295 K using pulsed photolysis/laser-induced fluorescence detection of the OH radical. A rate constant of $(0.99 \pm 0.05) \times 10^{-10}$ molecules^{-1} cm^3 s^{-1} at 20 Torr in argon was determined, which is consistent with previous results for the high-pressure limiting rate constant. We present the first experimental observation of the falloff region for this reaction and have modeled the pressure dependence of the rates using the Troe formalism. Canonical variational transition state theory calculations were performed on the basis of recent ab initio calculations to determine the relative branching among the four possible isoprene−OH adducts in the high-pressure limit. We find OH addition to the outer carbon positions dominates OH addition to the inner carbon positions. We have employed RRKM/master equation calculations to evaluate the pressure dependence of the overall rate and the rates for the individual isomers in the pressure range 0.25−1000 Torr. The excellent agreement between the calculated and experimental falloff behavior provides an independent test of the ab initio energetics and RRKM/ME treatment. The results shed light on the mechanisms for oxidation of isoprene in the troposphere.

Introduction

Isoprene (2-methyl-1,3-butadiene) is the major biogenic nonmethane hydrocarbon in the atmosphere. It is emitted by a wide variety of plants during daylight with a worldwide emission of ∼300−450 Tg/year[1] as a mechanism to protect plant membranes under conditions of extreme temperature and lack of water.[2] As much as 2% of the available carbon utilized in photosynthesis under ambient summer temperatures is fixed as isoprene.[3] The natural abundance of isoprene ensures that its tropospheric oxidation plays an important role in regional air quality. Since isoprene emission is primarily diurnal, the reaction with OH is the dominant initiation step in the tropospheric removal mechanism.

The first step in the oxidation of isoprene occurs predominantly via the addition of the hydroxyl radical, OH, to one of four sites, resulting in the four possible isoprene−OH adducts shown in Figure 1. Addition of OH to the outer carbons yields the allylic radicals labeled I and IV. Addition of OH to one of the inner carbons yields the primary radicals, labeled II and III. Although the oxidation of isoprene involves many subsequent reaction steps, the initial isomeric branching of the isoprene−OH adducts may strongly influence the final product distribution. Despite the importance of the initial step in the oxidation chemistry, there is no direct experimental evidence for the relative branching between the isomers. Peeters et al. have derived structure activity relationships from kinetic data for OH addition to simple hydrocarbons, but the predictions have yet to be critically tested.[4,5] Several models have been proposed for the complete oxidation mechanism, but there remains a notable lack of direct kinetic measurements of the intermediate processes. OH cycling experiments have provided indirect information on the intermediate processes, although many questions remain.[6,7] The oxidation of isoprene yields four major end products: methyl vinyl ketone, methacrolein, formaldehyde, and 3-methylfuran,[8−11] and Carter and Atkinson have recommended a ratio of 0.27:0.19:0.50:0.038, respectively.[12] In a mechanism proposed by Carter and Atkinson, isomer I yields methyl vinyl ketone, isomer IV yields methacrolein, and 3-methylfuran results from both isomers II and III. Formalehyde is formed as a coproduct from isomers I and IV. Recent theoretical calculations have challenged elements of this mechanism, suggesting that isomers I and II lead primarily to MVK and isomers III and IV yield methacrolein, requiring an alternative source of 3-methylfuran.[13]

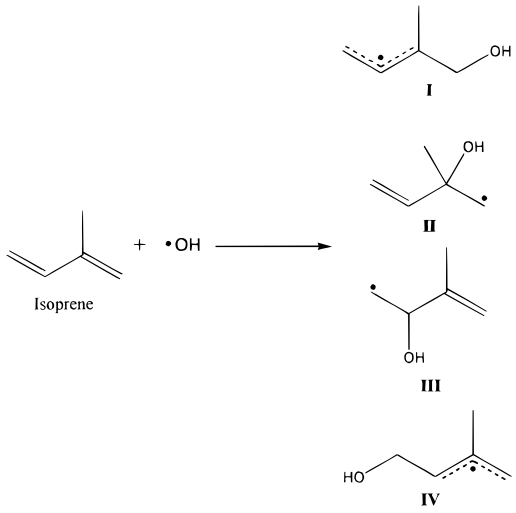

Figure 1. Reaction of isoprene with OH radicals.

[†] Department of Chemistry.
[‡] Department of Atmospheric Sciences.

10.1021/jp001163c CCC: $19.00
Published on Web 06/21/2000

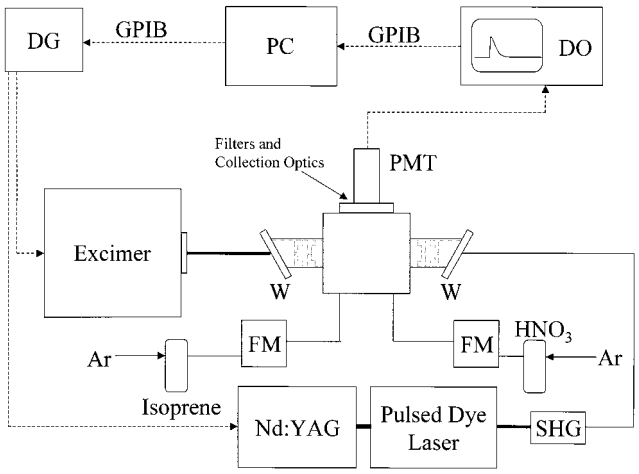

Figure 2. Schematic diagram of the experiment. Abbreviations in the figure are as follows: DG, delay generator; DO, digital oscilloscope; PC, personal computer; PMT, photomultiplier tube; W, window placed at Brewster's angle; FM, flow meter; SHG, second harmonic generator.

The high-pressure reaction rate for the addition of OH to isoprene has been determined previously,[6,7,14−18,25] and Atkinson has recommended a value of 1.01×10^{-10} molecules^{-1} cm^3 s^{-1} at 298 K.[19] The temperature dependence of the isoprene−OH reaction has also been measured, showing a weak negative dependence consistent with "barrierless" addition reactions.[6,15] Although addition reactions should exhibit a pressure dependence, there has been no previous experimental exploration of the OH−isoprene reaction in the low-pressure regime. A recent measurement has shown, however, that the reaction is still in the high-pressure limit in 2 Torr of helium.[7] Measurements of both the temperature and pressure dependence of addition reactions is important in atmospheric modeling to ensure that the reaction is effectively modeled for a range of altitudes and to provide a stringent test of the modeling results.

Preliminary theoretical results of the present study can be found elsewhere.[20] In the present report, we provide a more complete description of the theoretical results and details of the experimental determination of the pressure dependence. We have determined pressure-dependent rate constants for the reaction of isoprene with hydroxyl radicals at total pressures between 500 mTorr and 20 Torr using laser photolysis/laser-induced fluorescence (LP/LIF). Measured rate constants varied from $(0.76 \pm 0.08) \times 10^{-10}$ molecules^{-1} cm^3 s^{-1} at 500 mTorr to $(0.99 \pm 0.05) \times 10^{-10}$ molecules^{-1} cm^3 s^{-1} at 20 Torr. To permit facile modeling of the falloff regime, we have fit the pressure-dependent rate constants using the well-known two-parameter Troe form, resulting in rate constants of $k_0 = (6.9 \pm 2.2) \times 10^{-26}$ molecules^{-2} cm^6 s^{-1} and $k_\infty = (1.04 \pm 0.04) \times 10^{-10}$ molecules^{-1} cm^3 s^{-1}. We have also performed canonical variational transition state theory (CVTST) and Rice−Ramsperger−Kassel−Marcus/master equation (RRKM/ME) calculations using the results of recent high-level ab initio calculations on the four isoprene−OH adduct isomers. The calculations provide pressure-dependent branching ratios between the four possible isomers and reproduce the experimental falloff measurements. The mechanisms for isoprene oxidation are discussed in light of the present results.

Experiment

The experimental determination of the rate constants was performed using a recently constructed slow flow apparatus, shown schematically in Figure 2. The stainless steel reaction cell was evacuated by a high-throughput mechanical pump, and the pressure within the cell was monitored by a 1, 10, or 1000 Torr full scale capacitance manometer, depending on the total pressure. Isoprene (Aldrich, 99%), held at −15.0 °C, was buffered with argon and introduced through a flow meter. The total pressure over the mixture was measured using a 1000 Torr capacitance manometer, and the concentration was calculated using the known vapor pressure of isoprene.[21] Isoprene concentrations in the cell were typically less than 2×10^{15} molecules cm^{-3}. Hydroxyl radicals were produced by the photolysis of concentrated HNO_3 at 193 nm, which was introduced to the sample cell through a flow meter as a ∼5% mixture in argon. On the basis of the absorption cross section of HNO_3 at 193 nm and typical laser fluences, we estimate the concentration of OH radicals to be $\sim 5 \times 10^{10}$ molecules cm^{-3} in the probe volume. To minimize diffusion out of the probe region the photolysis volume always exceeded the probe volume. The photolysis of HNO_3 at 193 nm results in OH and O(^{1}D) products in approximately equal yields.[22] To assess the effects of the O(^{1}D) radicals on the measured rate, we have modeled the reaction kinetics, accounting for the collisional deactivation of O(^{1}D) by water and isoprene, hydrogen abstraction of O(^{1}D) from isoprene to form OH, and the reaction of O(^{1}D) with residual water from the concentrated HNO_3.[23,24] The O(^{1}D) radicals were effectively converted to OH in the reaction with water and had a negligible effect on the reaction rate after approximately 15 μs. In all cases, the OH concentrations were approximately 3 orders of magnitude lower than the isoprene concentrations, satisfying the pseudo-first-order approximation. The flow rates were adjusted to ensure that the molecules in the reaction zone were replenished between laser shots. Previous studies by Campuzano-Jost et al. have shown that isoprene may polymerize under static or very low flow conditions.[25] However, the flow rates used in the present study are sufficiently fast to ensure that polymerization will not affect the measured rate constants on the time scale reported by Campuzano-Jost et al. The reaction of NO_2 and HONO from the nitric acid photolysis with isoprene were not important due to the large excess of isoprene in the system.

The hydroxyl radical decay kinetics were measured using laser-induced fluorescence. The OH radicals were excited on the $Q_1(1)$ transition of the A ← X(1,0) vibrational band near 285.1 nm using the BBO-doubled output of a pulsed dye laser (LAS) running Rhodamine 575 pumped at 355 nm by a Nd:YAG laser (Spectra Physics GCR-150−10). The resulting fluorescence was collected through two 25 mm lenses and was detected by a photomultiplier tube (Hamamatsu R374). To reduce contributions from scattered light in the reaction cell, both BK7 and visible filters were placed in front of the collection optics, providing a band-pass filter near 300 nm that significantly decreased the contribution from scattered light from the photolysis and probe beams. The fluorescence decay was measured by a 400 MHz oscilloscope (Lecroy 9310A), and a finite region away from the scattered light signal was integrated and archived. The timing of the laser pulses was controlled by a digital delay generator (Stanford Research DG535), which was varied using GPIB control from a PC. The reaction kinetics were measured by storing the integrated fluorescence as a function of the delay between the photolysis and probe lasers. Typically, each fluorescence decay was averaged for 25 shots, and >100 time steps were taken with a step size between 0.25 and 1 μs. The OH decay curves were usually followed over 1 order of magnitude decrease in the integrated fluorescence signal. The probe laser power was adjusted to maintain saturation of the

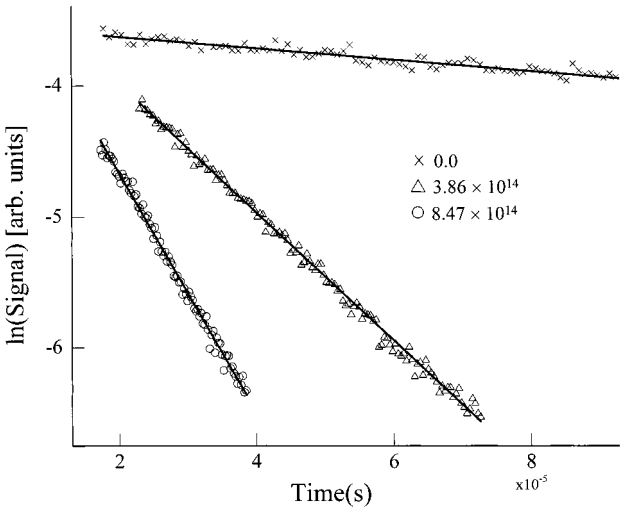

Figure 3. Log plots of the integrated fluorescence decay for a series of isoprene concentrations. The isoprene concentrations for each decay are shown in the figure and are given in molecules cm^{-3}.

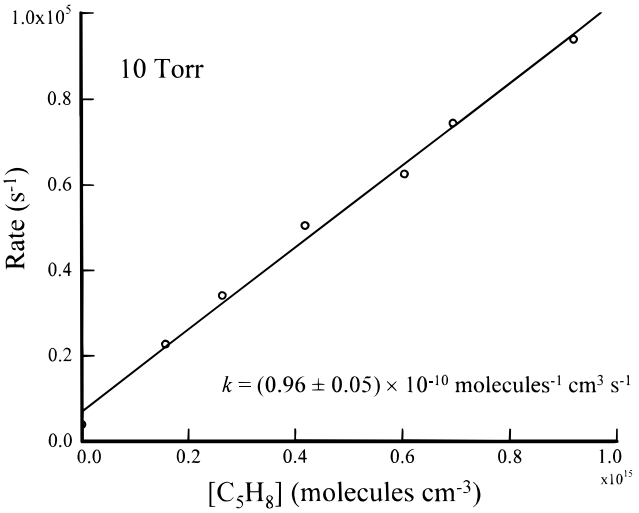

Figure 4. Bimolecular rate constant determination at 10 Torr.

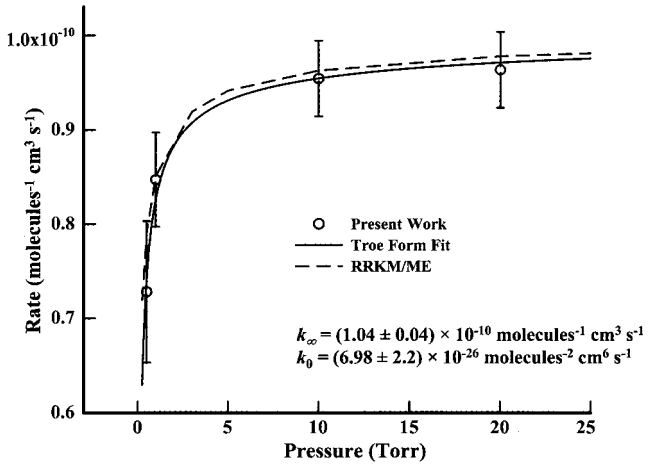

Figure 5. Experimentally determined pressure-dependent rate constants. The solid line represents a fit of eq 1 to the experimental data, and the dashed line represents the results of the RRKM/ME calculations.

OH transition. Temperatures in the reaction region were monitored using a chromel−alumel thermocouple with an error of ±1 K.

All errors in the present paper are 2σ errors from the linear least-squares fit to determine the bimolecular rates and provide a good estimate of the random error. Small systematic errors may arise due to the isoprene vapor pressure and photolysis of the isoprene by the 193 nm light. The error introduced from the vapor pressure is difficult to assess precisely, and such errors would be directly reflected in the rate constant. We have chosen to use the experimental enthalpy of vaporization to calculate the vapor pressures,[26] which shows a good fit to experimental vapor pressures over a temperature range of 207−307 K.[21] On the basis of an approximate absorption cross section of isoprene at 193 nm[27] and typical laser fluences, we estimate that approximately 1−2% of the isoprene will be photolyzed. Though these errors will affect the magnitudes of the reported rate constants, the relative rates will be unaffected, and we have chosen to report only the random error from the 2σ linear least-squares fit.

As a calibration of the apparatus, the reaction of ethane with OH was studied at 295 K. Pure ethane (Aldrich, 99+% purity) was introduced through a flow meter, and the concentrations were measured using a 10 Torr capacitance manometer. Typical concentrations of ethane were 1×10^{15} to 1×10^{16} molecules cm^{-3}, ensuring that the pseudo-first-order approximation was valid. A rate constant of $(2.5 \pm 0.2) \times 10^{-13}$ $molecules^{-1}$ cm^3 s^{-1} was measured, in good agreement with previous results.[23] No change in the rate constant with total pressure was observed, as expected for a direct abstraction reaction.

Results and Analysis

Experiment. Figure 3 shows typical data obtained for the first-order decay of the OH radical in the presence of isoprene. The log plots are linear over 1 order of magnitude change in the OH radical concentration, indicating that the pseudo-first-order approximation is valid under the experimental conditions of this study. The photolysis of HNO_3 results in OH radicals in a rotational distribution characterized by large rotational temperatures either by direct photolysis or by the reaction of $O(^1D)$ atoms with water.[28] We have examined the rotational relaxation of OH radicals under our experimental conditions by measuring LIF spectra of the Q_1 and R_1 branches of the $1 \leftarrow 0$ band as a function of delay time. Simulations of the spectra using available spectroscopic information allowed the rotational temperature to be estimated.[29] At early times, the rotational temperatures were near 700 K and were found to decrease significantly with increasing delay time. To ensure that only thermalized OH was measured and that the presence of $O(^1D)$ radicals had a negligible effect, kinetics were obtained by using a delay time offset >15 μs from the photolysis pulse. Figure 4 shows a typical pseudo-first-order decay plot. The plots are all linear with the isoprene concentration, indicating that the rotational distribution is thermalized and that the presence of $O(^1D)$ did not significantly affect the observed kinetics. Bimolecular rates were determined for a number of total pressures in order to quantify the pressure dependence of the rate constant. Figure 5 shows the pressure-dependent rate constants, along with a fit to the Troe expression of the form[23,30]

$$k([\mathrm{M}],T) = \frac{k_0(T)[\mathrm{M}]}{1 + k_0(T)[\mathrm{M}]/k_\infty(T)}\, 0.6^{\left\{1 + \left(\log \frac{k_0(T)[\mathrm{M}]}{k_\infty(T)}\right)^2\right\}^{-1}} \quad (1)$$

where [M] is the concentration of the buffer gas, $k_0(T)$ is the low-pressure termolecular rate constant, and $k_\infty(T)$ is the high-pressure limiting rate constant. The best fit k_0 and k_∞ values at

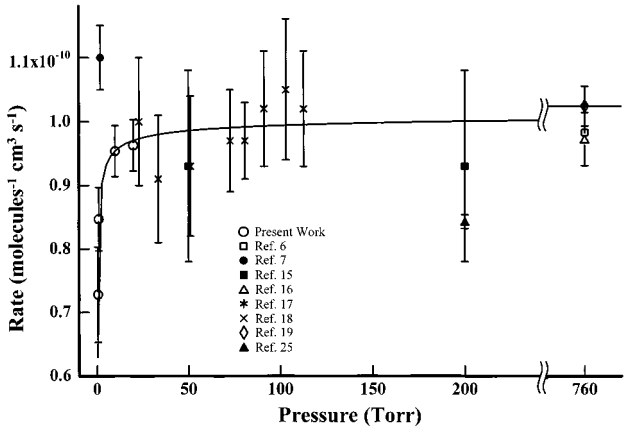

Figure 6. Experimentally determined rate constants for the reaction of isoprene with OH for total pressures ranging from 0.25 to 760 Torr. Individual symbols represent the reported rate constants from previous rate constant determinations and are shown in the figure.

TABLE 1: Pressure-Dependent Rate Constants for the Isoprene−OH Reaction at 295 K determined uing LP/LIF

pressure (Torr)	rate (molecules^{-1} cm^3 s^{-1})
20	$(0.96 \pm 0.05) \times 10^{-10}$
10	$(0.95 \pm 0.05) \times 10^{-10}$
1	$(0.85 \pm 0.06) \times 10^{-10}$
0.5	$(0.73 \pm 0.08) \times 10^{-10}$

295 K are $(6.9 \pm 2.2) \times 10^{-26}$ molecules^{-2} cm^6 s^{-1} and $(1.04 \pm 0.04) \times 10^{-10}$ molecules^{-1} cm^3 s^{-1} respectively. The individual pressure-dependent rate constants are shown in Table 1. For comparison to previous results, Figure 6 shows the results of a number of previous rate constant determinations as a function of total pressure. The results of the present study appear to be consistent with the previous results but outside the cited error bars of the two most recent experiments.[7,25]

Rate Constant Calculations. To calculate the relative branching between the four isomers and to examine the pressure dependence of these rate constants, two separate calculations were performed. The high-pressure rate constants for the dissociation of the isoprene−OH adducts were calculated using canonical variational transition state theory (CVTST). The pressure dependence of the dissociation rates were calculated using Rice−Ramsperger−Kassel−Marcus/master-equation (RRKM/ME) theory at a number of total pressures between 250 mTorr and 1000 Torr. In both cases, the dissociation rates were converted to the association rates via the equilibrium constant

$$\frac{k_{rec}}{k_{uni}} = K_{eq} = \frac{Q_{AB}}{Q_A Q_B} \exp\left(\frac{\Delta E}{kT}\right) \quad (2)$$

where Q_{AB} is the partition function of the adduct, Q_A and Q_B are the partition functions of the individual products, and ΔE is the zero-point corrected reaction energy.

CVTST calculations provide a method to calculate the high-pressure limiting rate constants for a dissociation reaction. The unimolecular rate is given by

$$k_{uni} = \frac{kT}{h} \frac{Q^{\ddagger}_{AB}}{Q_{AB}} \exp\left(-\frac{\Delta E}{kT}\right) \quad (3)$$

where $Q^{\ddagger}_{AB}$ is the partition function of the transition state with the vibrational frequency corresponding to the reaction coordinate removed, Q_{AB} is the partition function of the adduct, and ΔE is the zero-point corrected transition state energy relative to the adduct minimum. Since the addition of OH to the double bonds in isoprene proceeds without a barrier, the location of the transition state was determined variationally by minimizing the reaction rate as a function of the C−OH distance.

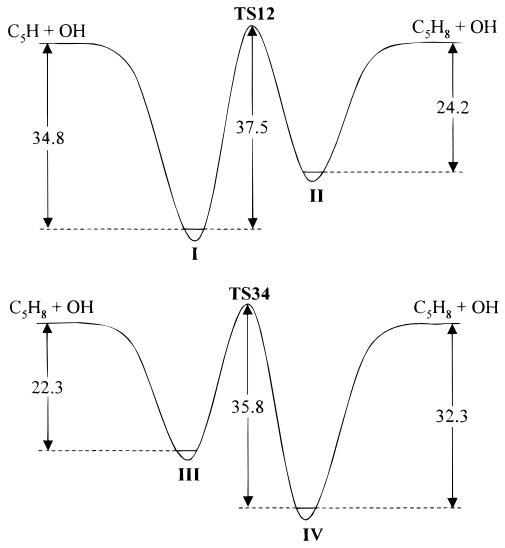

Figure 7. Schematic energy diagram (kcal/mol) for isomers of hydroxyisoprene radical including the isomerization pathways. The values are taken from ref 31.

The partition functions required for eqs 2 and 3 were calculated by treating the rotational and translational motion classically and treating vibrational modes quantum mechanically. Unscaled vibrational frequencies and moments of inertia were taken from recent ab initio calculations at the B3LYP/6-31G** level.[31] The reaction energies were taken to be zero-point corrected energies calculated at the CCSD(T)/6-311G**//B3LYP/6-31G** level. The relevant energies for the four isoprene−OH adducts including the transition states associated with interconversion of species II−I and III−IV are shown in Figure 7. The conserved modes of the transition state were assumed to resemble the product modes.[32] The dependence of the transitional mode frequencies with C−OH distance are modeled using[33]

$$\nu(r) = \nu_0 \exp[-a(r - r_e)] + B \quad (4)$$

where ν_0 is the vibrational frequency in the reactant molecule, r_e is the equilibrium bond distance, B is the sum of the rotational constants of the separate isoprene and OH molecules, and a is a constant. Moments of inertia at fixed geometries were calculated by changing only the C−OH distance. The potential energy surface along the reaction coordinate was modeled by the sum of a Morse function and centrifugal barrier,

$$V(r) = D_e[1 - \exp(-\beta r)]^2 + B_{ext}(r)J(J+1) \quad (5)$$

where D_e is the bond dissociation energy, $B_{ext}(r)$ is the external rotational constant determined by assuming that the molecule was a symmetric top,[39] and J was assumed to be the average rotational quantum number of a Boltzmann distribution calculated using the external rotational constant of the molecule at the equilibrium configuration.

We now briefly address the choice of a Morse function in the C−OH bond distance to model the reaction coordinate. It has been proposed that the potential along this coordinate is complicated, involving both a loose dipole−induced dipole complex and a barrier at shorter C−O bond lengths associated with a rehybridization of the carbon atom to form the covalent bond.[34] Abbatt and Anderson have provided a schematic view

of this potential for the addition of OH to ethylene, evaluating the energy of the van der Waals complex and inner transition state for conversion of the adduct to the complex. There is, however, evidence that the shape of the potential, in particular the height of the rehybridization barrier and the depth of the van der Waals well, is extremely sensitive to the level of the theory.[35] In the case of addition of Cl or F atoms to ethylene, studies employing a large-scale multireference configuration interaction treatment reported a marked decrease in the height of the transition state, which disappeared entirely for the F + C_2H_4 reaction at the highest levels of theory.[35,36] More recent calculations on the addition of OH to ethylene reveal a smooth monotonic increase in energy from the adduct minimum without a recombination barrier, and the authors were able to reproduce the experimentally measured activation energies.[37] We believe, therefore, that a Morse function should provide a reasonable description of the energy along the minimum energy pathway. The excellent modeling of the experimental falloff region and the very fast high-pressure rate constant for the reaction lends additional support for treating the reaction coordinate as a Morse potential. However, an accurate ab initio exploration would be preferable and should be pursued to find a more exact model for the reaction coordinate.

The individual rates of formation of each isomer were obtained using eqs 3 and 5, variationally minimizing the rate as a function of the C−OH distance for a given value of *a*. The individual rates were then summed, and the procedure was repeated for different values of *a* until the sum was equivalent to the recommended high-pressure limiting rate.[38] The value of *a* was determined to be 2.23 $Å^{-1}$. This value of *a* was then used to describe the translational mode frequencies for the subsequent RRKM/ME calculations.

The pressure dependence of the rate constants was modeled using the Rice−Ramsperger−Kassel−Marcus/master-equation (RRKM/ME) analysis, in which the rate constant for the dissociation of the adduct may be expressed by[39]

$$-k_{uni}g(E) = [\mathrm{M}]\int_0^\infty [R(E,E')\,g(E') - R(E',E)\,g(E)]\,\mathrm{d}E' - k(E)\,g(E) \quad (6)$$

where $g(E)$ is the population of the energy level with energy E, $[M]$ is the concentration of the buffer gas, and $R(E,E')$ is the rate of energy transfer from a level with energy E' to a level of energy E. The microcanonical rate constant at energy E, $k(E)$, is given by

$$k(E) = \frac{N^{\ddagger}(E - E_0)}{h\rho(E)} \quad (7)$$

where $N^{\ddagger}(E - E_0)$ is the sum of states at the transition state between energy E_0 and E, and $\rho(E)$ is the density of states of the reactant evaluated at energy E. Pressure-dependent rate constants are determined by weighting the microcanonical rate constants by the appropriate energy-level populations.

The UNIMOL suite of programs[40] was used for the RRKM/ME calculations of the rates in the falloff region. For the RRKM calculations, the transition state was assumed to be located at the same C−O bond length as used in the CVTST rate for all reaction energies. The moments of inertia, potential energy surfaces, and translational mode frequencies from the CVTST calculations were also used for the microcanonical calculations. The interaction between the bath gas and reactant molecule in the ME calculations was described by a Lennard-Jones potential,

$$V(r) = 4\epsilon\left[\left(\frac{\sigma}{r}\right)^{12} - \left(\frac{\sigma}{r}\right)^{6}\right] \quad (8)$$

where σ and ϵ are parameters describing the width and depth of the well, respectively. Since no experimental results are available for the interaction of the hydroxyisoprene radical and Ar, an approximate method described by Gilbert and Smith was used to determine collision parameters.[39] We have adopted values of $\epsilon = 233$ K and $\sigma = 4.74$ Å as the Lennard-Jones parameters.[41] To describe the collision energy transfer rate, Lennard-Jones collision integral corrections to the hard-sphere collision frequency were used to model the true collision frequency, and the energy transfer distribution was calculated by the biased random walk model[42] as implemented in the UNIMOL package. The collisional energy transfer parameters were assumed to be equal for all isomers.

High-pressure limiting rate constants for the formation of the four isomers are given in Table 2, along with the branching ratios in the high-pressure limit. Addition of OH to the end carbons is favored over the addition to the inner carbons. This is consistent with previous structure−activity relationship (SAR) estimates, although we find that the relative rates of formation of isomers II and III are significantly different. Pressure-dependent rate constants for the formation of the four possible isomers are shown in Figure 8. To allow the individual rates and product branching ratios to be evaluated easily, we have fit the pressure-dependent rates for the individual isomers using the two-parameter Troe form. The best-fit parameters are shown in Table 3. Though the fits are not quantitative at very low pressures, they provide a fair representation of the pressure-dependent behavior of the rate constants. The Troe parameters for isomers I and IV provide the best fit to the RRKM/ME calculations, differing by less than 5% for pressures down to 0.25 Torr.

The possibility of isomerization of the isoprene−OH adducts was also examined using RRKM/ME theory. Though the energies of adduct dissociation and isomerization are comparable, the transition state for isomerization is significantly tighter than the transition state for dissociation.[31] As a consequence, the calculated isomerization rates for the interconversion of the isomers via the transition states TS12 and TS34 were 3 orders of magnitude lower than the dissociation rates and will have a negligible effect on the total reaction rates reported. The temperature dependence of the rate constant was also examined using CVTST. Abstraction reactions, which exhibit a strong positive temperature dependence, can be effectively modeled using statistical rate calculations. Addition reactions that proceed without a barrier often show a slight negative temperature dependence that is poorly modeled using statistical theories even for relatively simply reactions such as the recombination of methyl radicals to form ethane.[43] In this study, we find a very weak positive temperature dependence, in contrast to previous experimental results.[6,15,19,25]

Discussion

The 20 Torr rate constant observed in this study, $k = (0.99 \pm 0.05) \times 10^{-10}$ molecules^{-1} cm^3 s^{-1}, is slightly lower than the high-pressure rate constant recommended by Atkinson. However, our data suggest that the 20 Torr rate lies near the beginning of the falloff regime, and the Troe-form fits provide a high-pressure rate, $k_\infty = (1.04 \pm 0.04) \times 10^{-10}$ molecules^{-1} cm^3 s^{-1}, that is consistent with the recommended high-pressure rate. To our knowledge, the experimental pressure-dependent rate constants determined in this study provide the first

TABLE 2: RRKM/ME Calculated High-Pressure Rate Constants for Hydroxyisoprene Radical Formation

isomer	rate of formation (molecules^{-1} cm^3 s^{-1})	branching ratio
I	5.58×10^{-11}	0.56
II	0.232×10^{-11}	0.023
III	0.456×10^{-11}	0.046
IV	3.71×10^{-11}	0.37
total	9.98×10^{-11}	

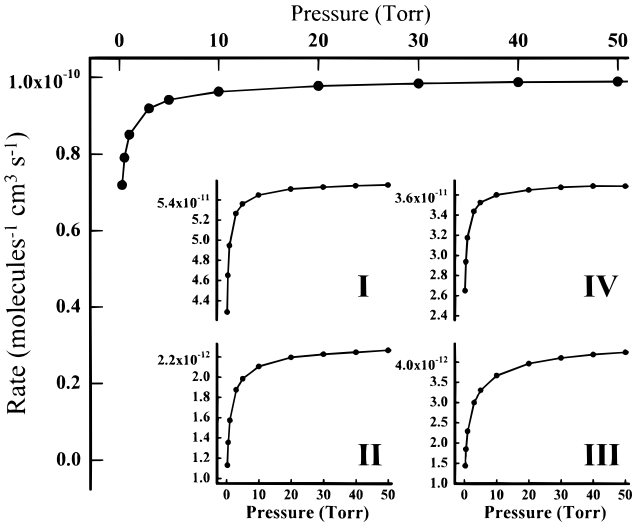

Figure 8. Computed rate constants as a function of pressure. The plot shows the sum of the rate constants for the individual isomers. The inset plots show the individual falloff curves for the four individual isoprene−OH adducts.

TABLE 3: Troe-Form Fitting Parameters for Results of RRKM/ME Calculations

isomer	k_0 (molecules^{-2} cm^6 s^{-1})	k_∞ (molecules^{-1} cm^3 s^{-1})
I	9.5×10^{-26}	5.8×10^{-11}
II	6.4×10^{-28}	2.4×10^{-12}
III	4.2×10^{-28}	4.7×10^{-12}
IV	4.1×10^{-26}	3.8×10^{-11}

exploration of the falloff regime for the OH−isoprene reaction. As shown in Figure 5, the present results are consistent with the majority of the previous rate constant determinations.

The present results, however, fall outside the error estimates for two recent rate constant determinations for the isoprene−OH reaction. The results of Stevens et al.[7] on the OH−isoprene reaction using LIF detection of the OH radical in a flow reactor are significantly higher than the present results. The authors determined a rate constant at 300 K in 2 Torr of He of $k = (1.10 \pm 0.05) \times 10^{-10}$ molecules^{-1} cm^3 s^{-1}, which is slightly higher than the recommended high-pressure rate. In the present study, however, we observe a rate constant at 295 K and 1 Torr of Ar of $k = (0.88 \pm 0.05) \times 10^{-10}$ molecules^{-1} cm^3 s^{-1}, indicating that the reaction is already in the falloff regime. To quantify the differences between the use of argon and helium as buffer gases, we have evaluated the isoprene−OH rate constant in 2 Torr of He using RRKM/ME calculations. The parameters from the CVTST calculations were used in the RRKM/ME calculations in 2 Torr of helium. Lennard-Jones parameters of $\epsilon = 69.0$ K and $\sigma = 4.28$ Å were used to describe the He−adduct interaction.[41] The calculated rate constant in 2 Torr of He at 298 K is 0.86×10^{-10} molecules^{-1} cm^3 s^{-1}. This rate constant is slightly smaller than the rate constant in Ar at 2 Torr and is significantly (>20%) lower than the rate measured by Stevens et al. A recent study by Hynes and co-workers on the reaction of OH with isoprene showed a rate constant of $(8.56 \pm 0.26) \pm 10^{-11}$ molecules^{-1} cm^3 s^{-1} at room temperature and a total pressure of 200 Torr that also differs from the present work.[25] In that study, the concentration of isoprene in the reaction chamber was measured by direct absorption of 228.1 nm light and was believed to be accurate to within the random error of the absorption measurement. The results of the present work differ by >20% from the results of Hynes and co-workers, though the origin of this discrepancy is unclear. Characterization of the isoprene concentration is a critical step in determining the rate constant. In a recent study of the isoprene + OH reaction in a flow reactor, Zhang, et al. calibrated the isoprene concentration by both the vapor pressure and a known He/isoprene mixture in a bulb. The observed rate constants were consistent and were observed to be $(10.2 \pm 0.9) \times 10^{-11}$ molecules^{-1} cm^3 s^{-1} at 112 Torr, consistent with the present results.[18]

The observed falloff provides a test of the applicability of the CVTST and RRKM/ME methodology used in this study. In addition, the ability of the RRKM/ME results to reproduce the experimental pressure dependence provides a measure of the accuracy of the ab initio data. To explore the sensitivity of the calculated falloff to the ab initio energetics, we have recalculated the pressure-dependent rates using well depths substantially larger and smaller than the calculated ab initio values. In both cases, the value of the parameter *a* was adjusted to give a final rate equivalent to the recommended high-pressure rate constant. The falloff characteristics of both sets of calculations were significantly different from the observed experimental rates and were unable to reproduce the experimental data. The large deviation observed for different well depths in addition to the quality of the fit using the ab initio energies and computational methodology of the present study is strong evidence that the calculations provide reasonable values for the pressure-dependent rate constants of each isomer.[20]

Structure activity relationships (SAR) have been previously utilized to determine the high-pressure branching ratios between the four isoprene−OH adducts. Peeters et al. have performed SAR studies for the addition of OH to a number of alkenes, including isoprene.[4,5] In the SAR method, site-specific rate constants are derived from available rate constant data based on whether the resulting adduct radical is primary, secondary, or tertiary. Delocalized radicals are represented by separate rate constants characterized by the nature of both radicals present in the set of resonance structures.[4] The derived site-specific rate constants were found to be consistent with fragmentation patterns in mass spectrometric studies of a number of asymmetric dienes.[5] For the addition of OH to isoprene, the relative isomeric branching using the SAR was found to be 0.60:0.05:0.05:0.30 for isomers I:II:III:IV. In general, the results of the present study are consistent with the previous SAR studies, though we find that the branching between isomers II and III differs significantly. This difference is due presumably to the presence of a methyl group on the active center in isomer II, which was not differentiated from the active center in isomer III in the SAR studies. The fraction of isomer IV was also found to be substantially larger in the present study than in the SAR studies, resulting primarily from a decrease in the relative branching to isomers II and III.

The calculated high-pressure branching ratios between the four OH−isoprene adducts can provide insight into the complete oxidation pathway for isoprene when compared to the available experimental information on the end product formation yields. Several different mechanisms containing many common features have been proposed for the complete tropospheric oxidation of isoprene and will be only broadly summarized.[12,13,44,45] Fol-

lowing OH addition to isoprene, the resulting hydroxyisoprene radical reacts with molecular oxygen under atmospheric conditions to form a hydroxyperoxy radical. The subsequent addition of O_2 to radicals II and III occurs only at the β-carbons but may occur at two centers (β or δ carbons) for radicals I and IV. Preliminary theoretical evidence indicates that addition of O_2 to the β-carbons is energetically favored, suggesting that the addition to isomers I and IV results in the formation of predominately β-hydroxyperoxy radicals.[46] In a recent study Jenkin and Hayman assumed that β-hydroxyperoxy radicals make up 75% of the total peroxy radical yield and were able to achieve good fits to their experimental absorption profiles.[44] For simplicity, the present results are discussed in terms of only the β-hydroxyperoxy radicals. In the presence of NO_x radicals, the β-hydroxyperoxy radicals are reduced to β-hydroxyalkoxy radicals through the removal of an oxygen atom. The resulting β-hydroxyalkoxy radical may react via three pathways: reaction with molecular oxygen, isomerization, and unimolecular dissociation. Recent ab initio calculations by Dibble have shown that the barrier to C−C bond cleavage between the α and β carbons is only ∼2 kcal/mol, suggesting that the unimolecular dissociation of the β-hydroxyalkoxy radical is the dominant process.[13] Based on Dibble's estimates, the rates of isomerization and reaction with molecular oxygen are expected to be several orders of magnitude lower than the unimolecular dissociation rate and will not contribute significantly to the observed end products.

Four major end products of the complete oxidation of isoprene have been identified in environmental chamber studies: methyl vinyl ketone (MVK), methacrolein (MACR), formaldehyde, and 3-methylfuran.[8−12] The recommended ratios for these species are 0.27:0.19:0.50:0.038, though unidentified peroxy nitrate species from the addition of NO make up 6−12% of the total end product yield and a number of unidentified carbonyl species are also present.[12] Tuazon and Atkinson initially proposed that MVK is formed primarily from isomers I and II and MACR from isomers III and IV, on the basis of the current knowledge of the oxidation end products.[10] Subsequent observation of a small fraction of 3-methylfuran[9] led to a number of proposed formation pathways. Carter and Atkinson have recently proposed that MVK is formed primarily from isomer I and MACR from isomer IV. Formaldehyde is formed from the subsequent oxidation of CH_2OH radicals formed as coproducts of MVK and MACR.[12] In the Carter and Atkinson mechanism, isomers II and III may each undergo cyclization reactions to form 3-methylfuran. The theoretical results of Dibble, however, suggest that the unimolecular dissociation occurs very quickly, implying that the cyclization pathway is relatively unimportant.[13] Formaldehyde is formed in addition to MVK and MACR, though it is formed directly from isomers II and III and is formed from the oxidation of CH_2OH by O_2 when derived from isomers I and IV. The observed 3-methylfuran end product is formed from a different source according to the theoretical results, possibly from the isomerization of the δ-hydroxyalkoxy radicals.[10] If we adopt the Carter and Atkinson mechanism and assume minimal subsequent isomerization, our results predict a ratio of 0.56:0.069:0.37 for MVK:3-methylfuran:MACR, which is consistent with the experimental end product yields. However, we find that our results are also consistent with the rapid decomposition of the β-hydroxyalkoxy radicals. If 3-methylfuran is not formed from the β-hydroxyalkoxy radicals, the ratio of MVK to MACR is predicted by our calculations to be 0.58:0.42, which is very close to the experimental ratio of 0.59:0.41. The similarity of the calculated results to these mechanisms suggests that the initial branching in the addition of OH to isoprene plays an important role in the final product branching ratios. However, the calculations are unable to distinguish between these mechanisms, and further work on the subsequent reaction steps is clearly necessary.

The pressure dependence of the rate constants may provide another avenue for elucidating the oxidation mechanism. The falloff curves for isomers II and III, shown in Figure 8, begin to decrease at much higher pressures than isomers I and IV. Isomer III shows the fastest decrease, and isomers I and IV show virtually identical pressure dependencies. These differences in the falloff behavior will have a subtle effect on the pressure-dependent branching between MVK and MACR, and detailed measurements of the end product branching ratios as a function of pressure may provide a method for differentiating the two mechanisms.

Conclusion

This work represents the first comprehensive study of the pressure dependence in the first step of the tropospheric oxidation of isoprene. The pressure-dependent rate constants for the reaction of isoprene with OH radicals have been determined using the LP/LIF technique. Transition state theory calculations have been performed to describe the relative isomeric branching ratios in the high-pressure limit, and RRKM/ME calculations have provided information on the pressure dependence of the individual isomers. These results indicate that the addition of OH to isoprene may play a major role in determining the end product yields.

In the future, we intend to extend both the experimental and computational aspects of this study to include the second step of the tropospheric oxidation mechanism, reaction of the hydroxyisoprene radical with O_2.

Acknowledgment. The authors thank Prof. Joaquin Espinosa-Garcia for helpful discussions. The authors would also like to thank Dr. Agnes Derecskei-Kovacs and Wenfang Lei for providing the ab initio results prior to publication. The authors gratefully acknowledge the reviewers for their helpful comments. The technical assistance of M. Clark Church is gratefully appreciated. This work was supported by an Interdisciplinary Research Initiative Grant from Texas A&M University and the Texas Advanced Research Program under Grant No. 010366-0306.

Note Added in Proof: We have become aware of two studies on the falloff behavior that have recently been published in this journal.[47,48] The k_0 values in the present study are consistent with the Arrhenius expression determined by Chuong and Stevens,[47] but the authors observed no pressure dependence below 343 K. The low pressure rate constants from the RRKM/ME calculations in the present work are consistent with the low pressure branching ratios calculated by Stevens et al.[48] However, the conclusion by Stevens et al. that the high pressure branching is equal for the four isomers is different from the present results.

References and Notes

(1) Brasseur, G. P.; Chatfield, R. B. In *Trace Gas Emission from Plants*; Sharkey, T. D., Holland, E. A., Mooney, H. A., Eds.; Academic Publishing: San Diego, 1991; p 1. Rasmussen, R. S.; Khalil, M. A. *J. Geophys. Res.* **1988**, *93*, 1417.

(2) Sharkey, T. D.; Singsaas, E. L. *Nature* **1995**, *374*, 769.

(3) Monson, R. K.; Fall, R. *Pl. Physiol.* **1989**, *90*, 267. Loreto, F.; Sharkey, T. D. *Planta* **1990**, *182*, 523.

(4) Peeters, J.; Boullart, W.; Hoeymissen, J. V. In *Proceedings of EUROTRAC Symposium '94*; Borrell, P. M., et al., Eds.; SPB Academic Publishing: The Hague, The Netherlands, 1994; p 110.

(5) Peeters, J.; Boullart, W.; Pultau, V.; Vandenberk, S. In *Proceedings of EUROTRAC Symposium '96*; Borrell, P. M., Borrell, P., Cvitas, T., Kelly, K., Seiler, W., Eds.; Computational Mechanics Publications: Southampton, 1996; p 471.

(6) Siese, M.; Koch, R.; Fittschen, C.; Zetzsch, C. In *Proceedings of EUROTRAC Symposium '94*; Borrell, P. M., et al., Eds.; SPB Academic Publishing: The Hague, The Netherlands, 1994; p 115.

(7) Stevens, P.; L'Esperance, D.; Chuong, B.; Martin, G. *Int. J. Chem. Kinet.* **1999**, *31*, 637.

(8) Gu, C. I.; Rynard, C. M.; Hendry, D. G.; Mill, T. *Environ. Sci. Technol.* **1985**, *19*, 151.

(9) Atkinson, R.; Aschmann, S. M.; Tuazon, E. C.; Arey, J.; Zielinska, B. *Int. J. Chem. Kinet.* **1989**, *21*, 593.

(10) Tuazon, E. C.; Atkinson, R. *Int. J. Chem. Kinet.* **1990**, *22*, 1221.

(11) Paulson, S. E.; Flagan, R. C.; Seinfeld, J. H. *Int. J. Chem. Kinet.* **1992**, *24*, 79.

(12) Carter, W. P. L.; Atkinson, R. *Int. J. Chem. Kinet.* **1996**, *28*, 497.

(13) Dibble, T. S. *J. Phys. Chem. A* **1999**, *103*, 8559.

(14) Cox, R. A.; Derwent, R. G.; Williams, M. R. *Environ. Sci. Technol.* **1980**, *14*, 57.

(15) Kleindienst, T. E.; Harris, G. W.; Pitts, J. N., Jr. *Environ. Sci. Technol.* **1982**, *16*, 844.

(16) Atkinson, R.; Aschmann, S. M.; Winer, A. N.; Pitts, J. N., Jr. *Int. J. Chem. Kinet.* **1982**, *14*, 507.

(17) Ohta, T. *J. Phys. Chem.* **1983**, *87*, 1209.

(18) Zhang, R.; Suh, I.; Clinkenbeard, A. D.; Lei, W.; North, S. W. *J. Geophys. Res.* **2000**, in press.

(19) Atkinson, R. *Int. J. Chem. Kinet.* **1996**, *28*, 731.

(20) Lei, W.; Zhang, R.; McGivern, W. S.; Derecskei-Kovacs, A.; North, S. W. *Chem. Phys. Lett.* **2000**, in press.

(21) Lide, D. R., Ed. *CRC Handbook of Chemistry and Physics*; CRC Press: Boca Raton, FL, 1996.

(22) Myers, T. L.; Forde, N. R.; Hu, B.; Kitchen, D. C.; Butler, L. J. *J. Chem. Phys.* **1997**, *107*, 5361.

(23) DeMore, W. B.; Sander, S. P.; Howard, C. J.; Ravishankara, A. R.; Golden, D. M.; Kolb, C. E.; Hampson, R. F.; Kurylo, M. J.; Molina, M. J. *Chemical Kinetics and Photochemical Data for Use in Stratospheric Modeling*; Evaluation 12; Jet Propulsion Laboratory: Pasadena, CA, 1997.

(24) Since the rates of reaction and collisional deactivation for isoprene + $O(^1D)$ are not known, we have used values of 2.0×10^{-10} molecules^{-1} cm^3 s^{-1} to describe both processes, which are consistent with rates of reaction and deactivation for $O(^1D)$ with other large hydrocarbons. Michaud, P.; Paraskevopoulos, G.; Cvetanovic, R. J. *J. Phys. Chem.* **1974**, *78*, 1457.

(25) Campuzano-Jost, P.; Williams, M. B.; D'Ottone, L.; Hynes, A. J. *Geophys. Res. Lett.* **2000**, *27*, 693.

(26) Cox, J. D.; Pilcher, G. *Thermochemistry of Organic and Organometallic Compounds*; Academic Press: New York, 1970.

(27) Jones, L. C.; Taylor, L. W. *Anal. Chem.* **1955**, *27*, 228.

(28) Jacobs, A.; Klainermans, K.; Kuge, H.; Wolfrum, J. *J. Chem. Phys.* **1983**, *79*, 3162.

(29) Luque, J.; Crosley, D. R. "LIFBASE: Database and Spectral Simulation Program (Version 1.5)," SRI International Report, MP 99-009, 1999.

(30) Troe, J. *J. Chem. Phys.* **1977**, *66*, 4745.

(31) Lei, W.; Derecskei-Kovacs, A.; Zhang, R., in preparation.

(32) The conserved mode frequencies were also modeled by allowing them to increase exponentially to the product frequencies. However, since the transition state is located far from the equilibrium bond distance, the difference from the product frequencies was found to be negligible.

(33) Hase, W. L. *Chem. Phys. Lett.* **1987**, *139*, 389.

(34) Abbatt, J. P. D.; Anderson, J. G. *J. Phys. Chem.* **1991**, *95*, 2382.

(35) Engels, B.; Peyerimhoff, S. D.; Skell, P. S. *J. Phys. Chem.* **1990**, *94*, 1267.

(36) Engels, B.; Peyerimhoff, S. D. *J. Phys. Chem.* **1989**, *93*, 4462.

(37) Villa, J.; Gonzalez-Lafont, A.; Lluch, J. M.; Corchado, J. C.; Espinosa-Garcia, J. *J. Chem. Phys.* **1997**, *107*, 7273.

(38) Atkinson, R. *J. Phys. Chem. Ref. Data* **1997**, *26*, 215.

(39) Gilbert, R. G.; Smith, S. C *Theory of Unimolecular and Recombination Reactions*: Blackwell Scientific: Oxford, U.K., 1990.

(40) Gilbert, R. G.; Smith, S. C.; Jordan, M. J. T. *UNIMOL program suite (calculation of falloff curves for unimolecular and recombination reactions)*, 1993. Available from the authors: School of Chemistry, Sydney University, NSW 2006, Australia or by e-mail to gilbert_r@summer.chem.su.oz.au.

(41) See ref 39 for details on approximating the Lennard-Jones parameters. To determine ϵ, the normal boiling point of the reactant molecule is required. We have chosen to use the boiling point of 2-methyl-3-butene-1-ol (393.7 °C), which is a closed-shell species analogous to radical I shown in Figure 1, to determine this parameter: Aldrich Chemical Co. *Catalog Handbook of Fine Chemicals*; Aldrich Chemical Co.: Milwaukee, WI, 1990.

(42) Lim, K. F.; Gilbert, R. G. *J. Chem. Phys.* **1986**, *84*, 6129.

(43) Hase, W. L.; Wardlaw, D. M. In *Advances in Gas-Phase Photochemistry and Kinetics: Bimolecular Collisions*; Ashfold, M. N. R., Baggott, J. E., Eds.; Royal Society of Chemistry: London, 1989; p 171.

(44) Jenkin, M. E.; Hayman, G. D. *J. Chem. Soc., Faraday Trans.* **1995**, *91*, 1911.

(45) Atkinson, R.; Arey, J. *Acc. Chem. Res.* **1998**, *31*, 574.

(46) Lei, W.; Derecskei-Kovacs, A.; Zhang, R.; McGivern, W. S.; North, S. W. Unpublished results.

(47) Chuong, B.; Stevens, P. S. *J. Phys. Chem. A* **2000**, *104*, 5230.

(48) Stevens, P. S.; Seymour, E.; Li, Z. *J. Phys. Chem. A* **2000**, in press.